Collapse of Xe polarized atomic states in magnetic fields

E. A Viktorov, M. Dimitrijević, V. A Srećković, N. N Bezuglov, K. Miculis, A. Pastor, P. Yu. Yu Serdobintsev

Collapse of Xe polarized atomic states in magnetic fields

E.A. Viktorov[1], M.S. Dimitrijević[2,3,1], V.A. Srećković[4], N.N. Bezuglov[1,5,6], K. Miculis[6], A. Pastor[1], P.Yu. Serdobintsev[1]

[1]*Saint Petersburg State University, 7/9 Universitetskaya nab., St. Petersburg,199034, Russia*
[2] *Astronomical Observatory, Volgina 7 11060, Belgrade 74, Serbia*
[3]*Sorbonne Université, Observatoire de Paris, Université PSL, CNRS, LERMA, F-92190, Meudon, France*
[4]*Institute of Physics Belgrade, UB, P.O. Box 57 11001, Belgrade, Serbia*
[5]*Rzhanov Institute of Semiconductor Physics SB RAS, 630090 Novosibirsk, Russia*
[6]*University of Latvia, Institute of Atomic Physics and Spectroscopy, LV-1586 Riga, Latvia*

Abstract. Ionization of two-photon excited states $5p^5(^2P_{3/2})6p[^3/_2, {}^5/_2]_2$, M=2 (*jl*-coupling) of xenon atoms by circularly polarized probe light was studied experimentally in a supersonic beam**.** The observed photoionization signals revealed oscillation structure due to the Larmor precession of atomic states in an external magnetic field. We derived analytical formulas for the photoelectron current and explained the diversity in the structure of the detected oscillations in terms of the principal lines among multiplet components of optical transitions. The obtained numerical data demonstrate collapse and revival (beating) behavior of the photocurrent due to nonlinearity of Zeeman shifts in the presence of the Paschen–Back effect. Our results indicate the possibility of implementing Doppler-free spectroscopy involving bound-free transitions.

1 Introduction

The analysis of temporal dynamics of fluorescence signals after excitation of atomic states by polarized light is an important area of modern spectroscopy [1]. Observation of magnetic resonances in polarized gas media is the basis of constructions and implementations of sensitive magnetometers [2, 3]. Applied controlled external magnetic fields result in diverse types of oscillating structures in detected fluorescence signals that allow making precision measurements of atomic state parameters beyond limitations due to Doppler broadening (Doppler-free spectroscopy) [1, 4, 5, 6]. Traditional methods of spectroscopy are associated mainly with bound-bound transitions with explicitly specified quantum numbers of the initial and final states involved into optical transitions. In the present report, we demonstrate, both experimentally and theoretically, a possibility to examine photocurrent oscillations at Larmor frequencies upon photoionization of polarized xenon atoms in a supersonic beam with polarised probe photons. Our experimental scheme has a number of important advantages compared with the detection of

[1] e-mail:mdimitrijevic@aob.rs

photons due to the almost 100% efficiency of extracting photoelectrons from the interaction zone. Probing excited gas media by photoionization methods allows, as well, to examine important details of nonlinear optical pump processes resulting in polarization of atomic states [7, 8]. We investigated cases of weak (linear Zeeman effect) and intermediate magnetic field values and revealed collapse and revival behaviour of oscillations in photocurrent signals as a result of the Paschen–Back effect [9, 10].

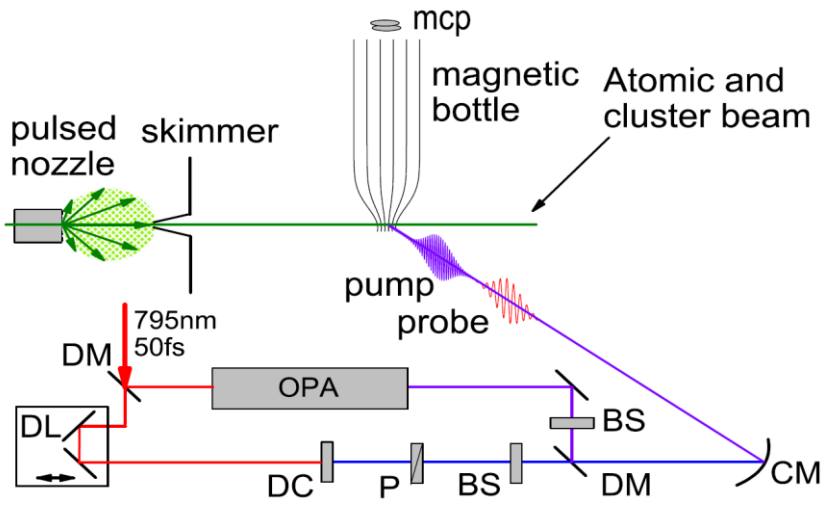

Figure 1. Experimental setup. OPA – optical parametric amplifier; DL – delay line; DM - dichroic mirrors; DC - doubling crystal; P – polarizer; BS - Babinet–Soleil compensators; CM – concave mirror.

2 Experimental setup

Xenon atoms were produced in a supersonic jet. A pulsed piezoelectric valve opens the bottle filled with mixture of xenon (8%) and helium gases under the pressure of 1 Bar into the vacuum chamber pumped out to 10^{-8} Torr. The velocity of Xe atoms in the supersonic flow was about 10^5 cm/sec. The supersonic jet passed the skimmer (see Fig. 1). After the skimmer the atoms in the ground unpolarized state crossed the focused laser beams. The Ti-Sapphire femtosecond laser PULSAR 10 (Amplitude Technologies, France) [11] has the following characteristics: main wavelength - 795 nm., pulse energy - 5 mJ, pulse duration - 50 fs, repetition rate - 10 Hz. The outcoming pulse was divided into two parts: (i) 70% of the pulse power pumped parametric amplifier TOPAS and was converted to UV radiation for 2-photon excitation of atomic states. (ii) The rest 30% of the power was used as probe radiation in the form of the second harmonic for ionization of pump-excited atoms. The correlation function of the pump (exciting) and probe (ionizing) pulses was measured by the signal of nonresonant multiphoton

ionization and amounted to 140 fs (FWHM). Circular polarization of both pump and probe pulses was performed using a Babinet-Soleil compensator.

Photoelectrons were trapped in an inhomogeneous magnetic field and their energy spectra were analysed by a magnetic-bottle time-of-flight electron spectrometer. In our experiments, the Teslameter PIE.MG R-2 magnetometer has measured the magnetic field value $B = |\vec{B}|$ equal to 0.825 (± 0.006) Tesla at the entrance to the magnetic bottle. The field orientation $\vec{e}_x = \vec{B}/B$ along x-axis was perpendicular to the quantization z-axis, which coincided with the direction $\vec{e}_z$ of the propagation of both laser beams.

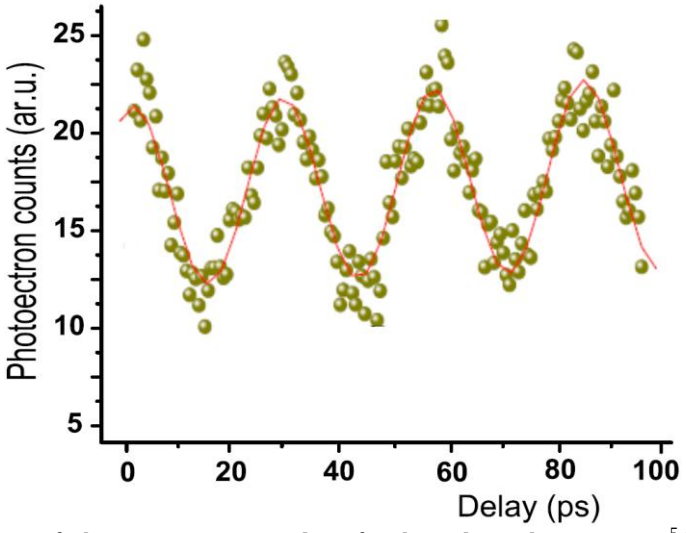

Figure 2. Delay dependence of photoionization signal I for the polarized Xe state $5p^5(^2P_{3/2})6p[^5/_2]_2$ (78120cm^{-1}), M=2. The points indicate the experimental data, while the solid curve corresponds to analytical results (Eqs. (4), (6), (7)) with the ratio of l-channels weights as 1: 3.4.

Two-photon excited states $5p^5(^2P_{3/2})6p[^5/_2]_2$ (78120cm^{-1}) and $5p^5(^2P_{3/2})6p[^3/_2]_2$ (79212,5cm^{-1}) (jl-coupling scheme [9]) of Xe atoms having the azimuthal (Zeeman) quantum number M=2 were produced by the femtosecond laser light (λ=256.01nm and 252.5nm) of the right circular polarization (see Fig. 1). Photoionization of the polarized atoms in the state with the total angular momentum J=2 and Zeeman component M=2 was operated as well by right-circularly polarized light of the second harmonic of titanium–sapphire laser (λ = 400 nm).

The delay time t between lasers pulses was varied in the range of 0 – 3 ns. With varying t, periodical oscillations of photocurrent pulses of intensity I (photo-signals) were arising (Figs. 2-3), as a result of the Larmor precession of the polarization moments of atomic states in the

magnetic field $\vec{B}$. This field-value along with the Larmor frequencies ω_L of the observed oscillations allowed us to determine Landé g-factors, both for the aforementioned excited state of the xenon atom using the well-known relation $\hbar\omega_L = g\mu_B B$ [2,9], where μ_B is the Bohr magneton. Figure 3 demonstrates the existence of both beatings in the registered signal and some relaxation process resulting in population depletion of the ionizing state with the decay constant $\tau \approx$ 6 ns. Theoretical consideration of the physics of experimental findings is presented in the next Section.

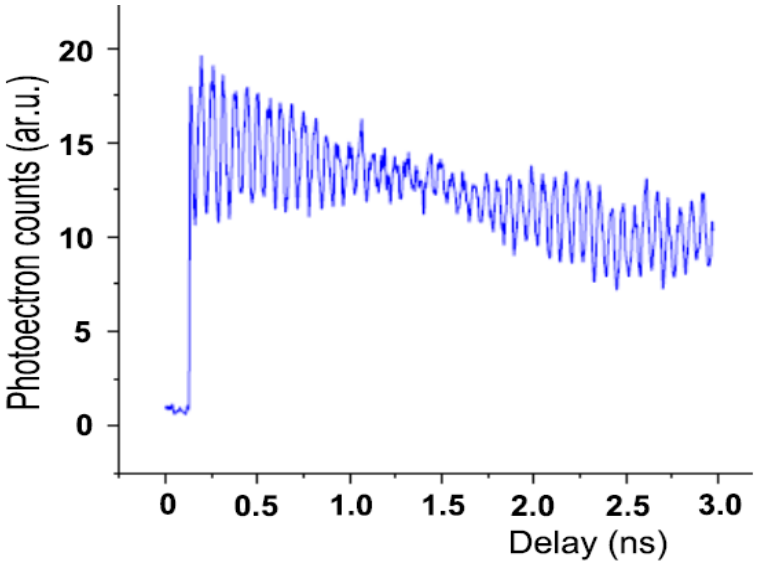

Figure 3. Delay dependence of photoionization signal I for the polarized Xe state $5p^5(^2P_{3/2})6p[^3/_2]_2$ (79212,5cm^{-1}), M=2.

3 Theoretical survey

Noteworthy, the conventional treaties of photoionization processes analyze the dependence of the observed photocurrent $I(t,\theta)$ on the angle θ between the laser beam and the escaping photoelectrons. Our experiment provides information on the aggregate electrons yield $I(t)$ averaged over all possible θ. In this Section we outline our theoretical study of the oscillation structure (see Figs. 2-3) in the photoionization signals $I(t)$ when polarized atomic states are ionized with circularly polarized photons from a laser beam. In what follows, we use the following notation: the azimuthal quantum numbers M along with the indices q of the polarization moments correspond to the "excitation coordinate system" with the quantization z-axis, while numbers M_x re-

fer to the system associated with the magnetic field, that is, with the x-axis as the quantization axis.

It is convenient to consider the effects of coherent interaction of polarized quantum particles with light in the framework of the technique of irreducible tensor operators for density matrices, which deals with the polarization moments of atoms ρ_q^κ and photons Φ_q^κ [1, 2, 4, 9].

3.1 Partial photoionization signals

An explicit expression for the photoionization cross-section σ was provided by authors of manual [1] (Section 20.2). In what follows, we will use their result in a slightly different form, which involves the photo-signal $I_{\Lambda,\Lambda'}(t)$

$$I_{\Lambda,\Lambda'}(t)/J_{ion} \sim D_0 M_0 \Phi_0^0 \rho_0^0(t) + D_1 M_1 \Phi_0^1 \rho_0^1(t) + D_2 M_2 \Phi_0^2 \rho_0^2(t)\,, \qquad (1)$$

and is more suitable for our purposes. Here J_{ion} is the intensity of the luminous flux of the ionizing probe laser. The indexes in $I(t)$ indicate the quantum numbers $\Lambda = 5s^2 5p^5 (^2P_j) nl[K]_J$ (*jl*-coupling scheme [9]) of the bound polarized atomic state in the initial channel and $\Lambda' = 5s^2 5p^5 (^2P_j) \varepsilon' l' [K']_{J'}$ ones in the final (ionization) channel with the notation ε' for the free photoelectrons energy. It is assumed that the quantum state ^2P_j of the atomic core remain unchanged due to the prohibition of intercombination transitions. Factors D_κ are expressed through 6*j*-symbols

$$D_\kappa = (-1)^{J+J'+1} \begin{Bmatrix} 1 & 1 & \kappa \\ J & J & J' \end{Bmatrix} |(\Lambda \| d \| \Lambda')|^2 \qquad (2)$$

and the reduced dipole matrix elements $(\Lambda \| d \| \Lambda')$ for bound-free optical transitions [1, 9]. Although the coefficients M_κ are trivial ($M_\kappa \equiv 1$) in the case of partial transitions, they play an important role in calculating the total photocurrent (see Eq. 5).

3.2 Zeeman shifts and density matrices temporal dependence

Effects of an interaction between atoms and magnetic fields are described in terms of Zeeman shifts [1, 9]. Due to the spin-orbit interaction, the state $\Lambda = 5s^2 5p^5 (^2P_j) nl[K]$ consists of two "fine" components $J = J_\pm = K \pm 1/2$ with the energy splitting $\Delta\varepsilon_K = \left|\varepsilon_{J_+} - \varepsilon_{J_-}\right|$. A detailed

description of Zeeman shifts $\Delta\varepsilon(M_x)$ in a coordinate system associated with the applied magnetic field (quantization x-axis) can be found in subsection 8.2 of book [9]. In our experimental conditions with comparatively weak magnetic fields, it is sufficient to restrict ourselves to considering of the linear and quadratic terms in $\Delta\varepsilon(M_x)$ over the Larmor frequency ω_L [9]:

$$\Delta\varepsilon(M_x)/\mathrm{h} = M_x\omega_L + \Theta\omega_L^2(J_+^2 - M_x^2);$$

$$\Theta = \left(\frac{2-g_K}{g_J}\right)^2 \frac{1}{\Delta\varepsilon_K/\mathrm{h}}\frac{1}{4J_+^2}. \qquad (3)$$

Here g_K and g_J denote Landé g-factors for the state $5s^25p^5(^2P_j)nl[K]$ and its "fine" component $5s^25p^5(^2P_j)nl[K]_J$ respectively.

The temporal dynamics of density matrices $\rho_{MM'}(t)$ and the relevant polarization moments $\rho_q^\kappa(t)$ in the presence of a magnetic field can be directly calculated using the Wigner rotation matrices [1, 12]. The latter provide a transformation between representations of an atomic density matrix associated with different quantization axes, which are directed along the magnetic field (x-axis) or laser beams (z-axis). In more general situations with several components (in our case, there are two of them) in a multiplet atomic state (as for the hyperfine components), it is preferable to numerically solve the Bloch equations for the density matrix based on, for example, the split propagation technique [13, 14].

If we are dealing with linear Zeeman shifts, there are simple explicit formulas for $\rho_{q=0}^\kappa(t)$ (see Appendix A). The first three atomic polarization moments ρ_0^κ with $\kappa = 0$ (population), $\kappa = 1$ (orientation) and $\kappa = 2$ (alignment) oscillate on zero, main ω_L and double $2\omega_L$ Larmor frequency:

$$\rho_0^0(t) = \rho_0^0(t=0); \quad \rho_0^1(t) = \cos(\omega_L t)\rho_0^1(t=0);$$

$$\rho_0^2(t) = (3\cos^2(\omega_L t) - 1)/2 \cdot \rho_0^2(t=0) \qquad (4)$$

3.3 Total photoionization signal

Expression (1) gives information on the partial cross section of photoionization when the quantum numbers l', K', J' in the final channel are fixed (i.e., measured). Since we did not separate the photoelectrons by l', K', J' numbers in the experiments, all the partial signals contribute

to the final cumulative photocurrent signal $I(t) = \sum_{\Lambda'} I_{\Lambda,\Lambda'}(t)$. Importantly, the sum rule for the product of three 6*j*-symbols (see Eq. (4.85) in [9]) makes it possible to perform explicit summation over the quantum numbers K' and J', provided that quantum defects of final states in the energy continuum are independent on K', J'. Omitting somewhat tedious algebraic calculations, we present the final result: $I(t) = I_{l'=l+1} + I_{l'=l-1}$, where two remaining partial signals $I_{l'}$ relate to escaping a free photoelectron with two possible values $l' = l \pm 1$ of its orbital quantum number. The ratio $I_{l'} / J_{ion}$ is expressed by a formula similar to that included in Eq. (1), with the following coefficients

$$D_\kappa = \begin{Bmatrix} 1\,1\,\kappa \\ l\;l\;l' \end{Bmatrix} |(nl \| d \| \varepsilon' l')|^2;$$

$$M_\kappa = (2J+1)(2K+1) \begin{Bmatrix} K\;K\;\kappa \\ J\;J\;1/2 \end{Bmatrix} \begin{Bmatrix} l\;\;l\;\kappa \\ K K\;j \end{Bmatrix} (-1)^{J+0.5-l-j} \qquad (5)$$

4 Results and discussion

Our main result boils down to the statement that the observed photocurrent signal $I(t)$

$$I(t) = \sum_{l'=l\pm1} \chi_{l'} I_{l'}(t); \qquad \chi_{l'} = (nl \| d \| \varepsilon' l')^2 \qquad (6)$$

is obtained as the sum of two partial signals $I_{l'}(t)$

$$I_{l'}(t) = I_0 \cdot \sum_{\kappa=0}^{2} D_\kappa M_\kappa \Phi_0^\kappa \rho_0^\kappa(t), \qquad (7)$$

statistical weights $\chi_{l'}$ of which are determined with the reduced dipole matrix elements (6) of bound-free optical transitions of the valence electron. The multiplier I_0 depends on intensities of applied lasers and experimental set-up parameters.

It is important to note that immediately after the excitation process at time $t = 0$, the angular momentum vector $\vec{J}(t=0)$ of the two-photon excited atomic state Ψ_i is directed along the wave vector (quantization z-axis) of the probe photons. The angular momentum $\vec{S}_{ph}$ of the photons (photon spin) has a unity value and is also directed along the z-axis. Upon the ionization at time *t*, the atom acquires the photon spin, i.e.

$$\vec{J}(t) \to \vec{J}' = \vec{J}(t) + \vec{S}_{ph} \qquad (8)$$

Table 1. Photon and atomic polarization moments.

	$\kappa = 0$	$\kappa = 1$	$\kappa = 2$
Φ_0^κ	$1/\sqrt{3}$	$1/\sqrt{2}$	$1/\sqrt{6}$
$\rho_0^\kappa(t=0)$	$1/\sqrt{5}$	$\sqrt{2}/(\sqrt{5})$	$\sqrt{2}/(\sqrt{7})$

4.1 Partial signals $I_{l'}(t)$

We first consider the features of photoionization signals $I_{l'}(t)$ in two outgoing channels $l = 1 \to l' = 1 \pm 1 = 0, 2$ when the polarized Xe states $\Psi_i = |P_{3/2}6p[3/2,5/2]_2, M = 2\rangle$ are ionized by the right-circularly polarised probe photons. The corresponding photonic and atomic polarization moments are expressed via Wigner 3*j* symbols [1]

$$\rho_0^\kappa(t=0) = \sqrt{2\kappa+1}\begin{pmatrix} J & J & \kappa \\ M & -M & 0 \end{pmatrix}; \qquad \Phi_0^\kappa = \sqrt{2\kappa+1}\begin{pmatrix} 1 & 1 & \kappa \\ 1 & -1 & 0 \end{pmatrix} \quad . \qquad (9)$$

with the numerical values shown in Table 1 (*J*=2, *M*=2).

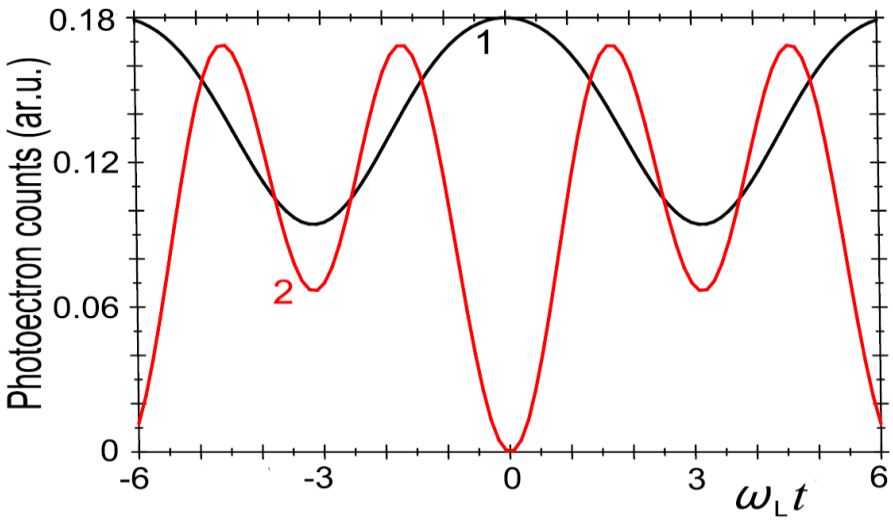

Figure 4. Temporal dependence of the partial photoionization signals $I_{l'}(t)$ (7) in two outgoing channels *l*'=2 (curve 1) and *l*'=0 (curve 2). The case of linear Zeeman shifts. The initial polarized atomic state is $P_{3/2}6p[^3/_2]_2$, *M*=2

Figure 4 shows the oscillation structure of partial photoionization signals $I_{l'}(t)$ (7) in the case of a weak magnetic field (linear case). It reveals both the shift between the calculated photocurrent oscillations and quite different shapes. The nature of these findings is due to the existence of the so-called principal lines (see subsection 9.2.3 of [9]) with the highest intensities among multiplet components of optical transitions. The most intense (principal) lines turn out to be those for which the change in *l*, *K*, and *J* is the same. Photoionization of the Ψ_i-state $P_{3/2}6p[3/2]_2$ with electrons escaping in the channel $l=1\rightarrow l'=2$ corresponds to the dominant transition $K=3/2\rightarrow K'=5/2$; $J=2\rightarrow J'=3$ for the multiplet $P_{3/2}6p[3/2]_2\rightarrow P_{3/2}\varepsilon' l'[K']_{J'}$. It means that two vectors with lengths 2 ($\vec{J}$) and 1 ($\vec{S}_{ph}$) after addition (8) yield a vector of length 3 ($\vec{J}'$), i.e. $\vec{J}$, $\vec{S}_{ph}$ should be directed along the same z-axis. The latter is realized at the moment $t_m=0$ of Ψ_i-state excitation. Because of the Larmor precession, the atomic vector $\vec{J}$ rotates around the magnetic field vector (x-axis), so that its vector sum $\vec{J}'$ (8) with the constant spin vector $\vec{S}_{ph}$ begins to decrease in length. This leads to dropping the probability of the dominant transition $J=2\rightarrow J'=3$ and a weakening of the photoionization signal $I_{l'=2}(t)$ (see plot 1 in Fig. 4). In the case of the channel $l=1\rightarrow l'=0$, another transition $K=3/2\rightarrow K'=1/2$; $J=2\rightarrow J'=1$ is formally associated with the dominant one. Small values of $K'=1/2$, and $J'=1$, however, essentially diminish the corresponding oscillator strength, making the so called satellite component [9] $K=3/2\rightarrow K'=3/2$; $J=2\rightarrow J'=2$ more intensive. There are two moments t_m within the Larmor period, when the spatial orientation of the vectors $\vec{J}$, $\vec{S}_{ph}$ in Eq. (8) does not change the length of $\vec{J}$:

$$J(J+1)=J(J+1)+2\sqrt{J(J+1)S_{ph}(S_{ph}+1)}\cos(\omega_L t_m)+S_{ph}(S_{ph}+1) \qquad (10)$$

The solutions $\omega_L t_m=\arccos(-1/(2\sqrt{3}))=\pm 1.863$ of Eq. (10) for $J=2, S_{ph}=1$ are in excellent agreement with the data of graph 2 in Fig. 4.

Figure 5 demonstrates dramatic changes in the dynamics of partial signals $I_{l'}(t)$, when, due to the Paschen - Back effect, the nonlinear term in the Zeeman shifts (3) leads to the collapse and subsequent retrieval of the polarized moments $\rho_0^{\kappa}(t)$ of the ionizing Ψ_i-state of Xe atom.

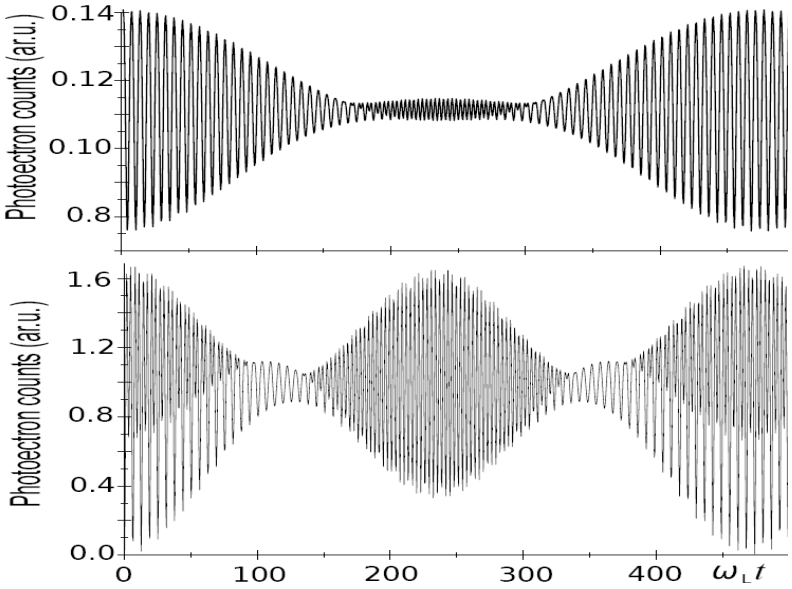

Figure 5. Same as in Fig. 4 in two outgoing channels *l*'=2 (upper frame) and *l*'=0 (lower frame) when the applied magnetic field results in the Paschen–Back effect. The value of the dimensionless parameter $\Theta \cdot \omega_L$ is 1/150 (see Eq. (3)).

4.2 Aggregated signal $I(t)$

The calculated values of the aggregated photoionization current *I* (6) are shown in Fig.2 (solid curve). A good agreement between the theoretical predictions and the experimentally obtained photoelectron signals can be seen provided that the ratio $\chi_{l'=3} / \chi_{l'=1}$ of the statistical weights is chosen equal to 3.3. The latter value corresponds to the Bethe rule [9, 15, 16], which ascribes a dominant role to photo-processes with the highest possible value of the orbital moment l' of the escaping photoelectrons.

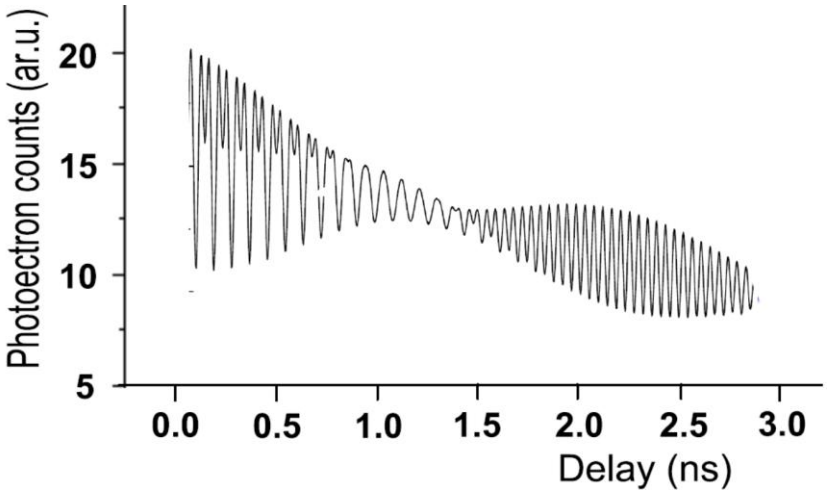

Figure 6. Same as in Fig. 3 for the aggregate photosignal $I(t)$ (6). Our numerical results are obtained for the following parameters: the product $\Theta \cdot \omega_L$ = 1/100, the ratio $\chi_{l'=3} / \chi_{l'=1}$ =3.1 and the relaxation constant τ = 6 ns.

We also performed numerical simulations to describe the experimental signal depicted in Fig. 3. The calculated photocurrent $I(t)$ temporal evolution is shown in Fig. 6. Signal fading was taken into account by introducing the decay fitting function: $I(t) \to \exp(-t/\tau) I(t)$ with the decay constant τ =6 ns. Satisfactory agreement between experimental and theoretical results can be observed. The formation of a beat structure in the signal $I(t)$ is clearly seen as a result of a nonlinear quadratic response in the Zeeman energy shifts.

Two well-known processes, that can contribute to the attenuation of the detected photocurrent, do not explain, however, the small value of the fitting parameter τ. (i) The natural lifetime of Xe $5p^5(^2P_{3/2})6p[^3/_2]_2$ state is ~ 27 ns while (ii) the decay time, corresponding to the transit time depletion [17] due to the escape of moving Xe atoms from the volume of the probe laser beam, turns out to be an order of magnitude larger. On the other hand, the magnitude of the applied magnetic field is not sufficient to obtain the fitting value $\Theta \cdot \omega_L$ = 1/100, necessary for the appearance of beats. This means that both the damping and the observed beats in the experimental signal in Fig. 3 have additional physical sources due, for example, to the rich isotopic composition of the Xe samples we use. Landé g-factors values for different isotopes can vary within 3%. From the point of view of a formal mathematical description, the role of these variations in phase decoherence processes is similar to nonlinear Zeeman shifts and will be analyzed in our future publication.

5. Conclusion

This paper presents experimental and theoretical studies of photoionization processes with the participation of two-photon excited states of Xe atoms in the presence of a magnetic field. The experimental setup did not distinguish between extracting photoelectrons in terms of quantum numbers and scattering angles. The observed temporal dynamics of the photocurrent revealed, nevertheless, an oscillatory structure due to the preparation of ionizing atoms in strongly polarized states, which are affected by the Larmor precession. We derived analytical formulas for the photocurrent explaining the variety of forms of recorded oscillations. The numerical data carried out demonstrate characteristic beats in oscillations (collapse followed by revival) due to the quadratic nonlinearity in the Zeeman shifts. We would like to emphasize the possibility of observing the effects of coherent quantum states interference (in our case, photocurrent oscillations) in the energy continuum. This allows, in particular, the realization of Doppler- free spectroscopy involving bound-free transitions. Additionally, such studies may be of interest and for magnetic star atmospheres investigations, where xenon is present and its spectral lines were observed. We note as well that such investigations may be of interest and for tokamak plasma where xenon may be added as impurity.

Acknowledgements

This work was supported by the Latvian Science Council Grant No lzp-2019/1-0280 and by the Russian Science Foundation under the grant No 18-12-00313 in the part regarding the theoretical analysis of photoionization signals observed in experiments with Xe atoms. The equipment of the Resource Center “Physical Methods of Surface Investigation” of the St. Petersburg State University was used in experiments. We thank Professor M. Auzinsh for useful discussions on issues related to our work.

Author contribution statement

All authors contributed equally to the paper.

Appendix A. Temporal dependence of polarization moments $\rho^{\kappa}_{q=0}$

If we restrict ourselves to the effects of linear Zeeman shifts, we can independently study the evolution of the polarization moments of atoms $\rho_q^\kappa(t)$ ($q=-\kappa,-\kappa=1,...,\kappa$) arising from the Larmor precession of the atomic angular momentum $\vec{J}$. The ρ_0^0 moment describes excited states population and is not affected by a magnetic field $\vec{B}$, i.e. ρ_0^0 does not depend on t.

In the "excitation coordinate system" (quantization z-axis), three components $\rho_q^1(t)$ correspond to spherical components $J_{0,\pm}$ of the vector $\vec{J}(t)$ [1,4] which is initially oriented along the unit vector $\vec{e}_z$ (see discussion regarding Eq. (8)). In other words $\rho_\pm^1(t=0)=0$ while $\Lambda\rho_0^1(t=0)\equiv J_0=J_z=\mid\vec{J}\mid$ (Λ is some constant depending on the excited states parameters). The vector $\vec{J}$ precession around the magnetic field (x-axis) results in $\Lambda\rho_0^1(t)\equiv J_z(t)=\mid\vec{J}\mid\cos(\omega_L t)$ (compare with Eq. (4)).

In the case of the alignment moments ($\kappa=2$), let's construct two matrix operators $\hat{T}(t)$ and $\hat{F}$. The first one $T_{qq'}(t)$ is proportional to the product of the vector $\vec{J}(t)$ spherical components $T_{qq'}=J_q J_{q'}$, while the second immutable matrix $F_{qq'}$ is formed by the product of the spherical components of the unit vector $\vec{e}_z$: $F_{qq'}=\delta_{q0}\delta_{q'0}$, where δ is the Kronecker delta function. In the next step, we consider the trace of the matrix product:

$$tr(\hat{T}(t)\hat{F})=\sum_{qq'}T_{qq'}F_{q'q}=\left|J_z(t)\right|^2=\mid\vec{J}\mid^2\cos^2(\omega_L t)\,. \qquad \text{(A1)}$$

On the other hand, the trace can be viewed as the scalar product of the involved matrices [9], i.e. the trace may be written in terms of their irreducible tensor operators [1,9]:

$$tr(\hat{T}(t)\hat{F})=\sum_{\kappa,q}T_q^\kappa F_{-q}^\kappa(-1)^q=\sum_{\kappa=0,2}T_0^\kappa F_0^\kappa=\mid\vec{J}\mid^2/3+T_0^{\kappa=2}(t)F_0^{\kappa=2}\,, \qquad \text{(A2)}$$

where we account for the following equalities: $T_0^{\kappa=0}=\mid\vec{J}\mid^2/\sqrt{3}$, $F_0^{\kappa=0}=1/\sqrt{3}$, $F_q^{\kappa=1}\equiv 0$, $F_{q\neq 0}^{\kappa=0}\equiv 0$ [1]. The comparison of Eq. (A1) with Eq. (A2) yields the temporal dependence

$$T_0^{\kappa=2}(t)F_0^{\kappa=2}=\mid\vec{J}\mid^2(\cos^2(\omega_L t)-1/3)\,, \qquad \text{(A3)}$$

presented in Eq. (4), for the atomic polarization moment $\rho_0^{\kappa=2}\sim T_0^{\kappa=2}$.

References

1. M. Auzinsh, D. Budker, and S. Rochester. *Optically Polarized Atoms*. *Understanding light-atom interactions*. Oxford University press, 2010.
2. E.B. Alexandrov, M. Auzinsh, D. Budker, D.F. Kimball, S.M. Rochester, and V.V Yashchuk. Journal of the Optical Society of America B. **22**, 7 (2005). https://doi.org/10.1364/JOSAB.22.000007
3. D. Budker & M. Romalis, Nature physics, **3**(4), 227-234 (2007). https://doi.org/10.1038/nphys566
4. E.B. Alexandrov, M.P. Chaika, and G.I. Khvostenko. *Interference of Atomic States*. Springer Series on Atoms and Plasmas; **7**, Springer-Verlag, Berlin, 1993.
5. D. Budker, D.Kimball, D. F. Kimball, & D. P. DeMille, Atomic physics: an exploration through problems and solutions. Oxford University Press, USA 2004.
6. M. Quack & F. Merkt, (Eds.). Handbook of high-resolution spectroscopy. Wiley-Blackwell 2011.
7. N. Porfido, N.N. Bezuglov, M.Bruvelis, G.Shayeganrad, S. Birindelli, F.Tantussi, I. Guerri, M. Viteau, A. Fioretti, D. Ciampini, M. Allegrini, E. Arimondo, A. Ekers, and F. Fuso. Phys. Rev. A. **92**, 043408 (2015). http://journals.aps.org/pra/abstract/10.1103/PhysRevA.92.043408.
8. H. R. Noh Symmetry, **8**(3), 17 (2016). https://doi.org/10.3390/sym8030017
9. I. Sobelman. *Atomic Spectra and Radiative Transitions*, volume 12 of Springer Series on Atoms+Plasmas. Springer Berlin Heidelberg, 1992.
10. C. J. Foot, Atomic Physics, Oxford masters series 2005.
11. Amplitude Technologies, France https://amplitude-laser.com
12. Landau, L. D. and Lifshitz, E. M. *Quantum Mechanics: Non-Relativistic Theory*. Pergamon Press, Oxford, 3d ed, 1977
13. I. Sydoryk , N.N. Bezuglov, I.I. Beterov, K. Miculis, E. Saks, A. Janovs, P. Spels, A. Ekers. Phys.Rev.A **77**, 042511 (2008). DOI: https://doi.org/10.1103/PhysRevA.77.042511
14. D. Efimov, (2010). Numerical simulation of dynamical chaos regime for Rydberg atoms based on the Split Propagation Technique. In Proceedings of International conference «Science and Progress» (pp. 237-241) 2010
15. A. B. Migdal. *Qualitative Methods in Quantum Theory*. Advanced Books Classics. Westview Press, 2000.
16. H. A. Bethe & E. E. Salpeter, *Quantum mechanics of one-and two-electron atoms*. Springer Science & Business Media (2012).
17. M. Bruvelis, J. Ulmanis, N.N. Bezuglov, K. Miculis, C. Andreeva, B. Mahrov, D. Tretyakov, and A. Ekers. Phys.Rev.A **86**, 012501 (2012).

https://doi.org/10.1103/PhysRevA.86.012501.